JOURNAL OF GEOPHYSICAL RESEARCH, VOL. 87, NO. C6, PAGES 4148–4154, MAY 20, 1982

# Evidence for the Influence of Form Drag on Bottom Boundary Layer Flow

T. M. CHRISS[1] AND D. R. CALDWELL

*School of Oceanography, Oregon State University, Corvallis, Oregon 97331*

An experiment in 199 m of water on the Oregon shelf produced continuous current speed profiles down to the sediment-water interface. These profiles show that the velocity structure above the viscous sublayer is consistent with that expected when form drag influences the boundary layer flow. They show two logarithmic-profile regions, each yielding a different stress estimate. The stress calculated from the upper one reflects the influence of form drag and is more than 4 times the bed stress determined frm the shear in the viscous sublayer. When form drag is significant, the application of logarithmic profile or Reynolds stress techniques to measurements more than a few tens of centimeters from the bed may yield bed stress estimates inappropriate for use in near-bed sediment transport or entrainment calculations. Large roughness-length or drag-coefficient values do not prove that a viscous sublayer does not exist.

## INTRODUCTION

In sediment transport studies it is important to distinguish between the contribution of skin friction and that of form drag to the total boundary stress [*Einstein*, 1950, 1964; *Smith*, 1977]. Skin friction here refers to the shear stress averaged over a few tens of grain diameters, whereas form drag is that portion of the total stress caused by the irregularity of the boundary. Although flow in the upper part of the boundary layer is influenced by the total stress, erosion and near-bed sediment transport are related to skin friction alone. When form drag is significant, the simple logarithmic profile expected in turbulent flow over a horizontally homogeneous surface may not be found. Instead, above a bed with sparse roughness elements the profile may consist of several regions with different logarithmic slopes [*Arya*, 1975]. In the outer region the mean flow is expected to obey the usual logarithmic law,

$$\bar{U}(z) = (U_*/k) \ln (z/Z_0) \quad (1)$$

where $k$ is von Karman's constant, $Z_0$ is a large-scale roughness parameter reflecting the influence of both small-scale topography and skin friction, and $U_* = (\tau_t/\rho)^{1/2}$ is a friction velocity based on the total stress $\tau_t$. Closer to the boundary, an internal boundary layer may develop in which the mean profile is also logarithmic

$$\bar{U}(z) = (u^*/k) \ln (z/z_0) \quad (2)$$

but where the friction velocity $u_*$ and the roughness parameter $z_0$ now reflect the characteristics of the surface between the large-scale roughness elements. This friction velocity $u_*$ is based on the local skin friction (which may be spatially variable) rather than on total stress. (If the intervening surface is hydrodynamically smooth, $z_0$ is not determined by the small-scale roughness characteristics, but rather by the thickness of the viscous sublayer [*Chriss and Caldwell*, 1981].) Although this description suggests a profile composed of two intersecting segments, *Smith* [1977] and *Smith and McLean* [1977] demonstrate that multiple roughness scales can generate velocity profiles with more than two segments. Thus when form drag is important the constant-stress assumption will not be valid.

In an earlier paper [*Caldwell and Chriss*, 1979], we demonstrated the existence of the viscous sublayer in the bottom boundary layer and found a logarithmic layer above it. In examining additional data from the experiment, segmented profiles were found in the logarithmic region (Figures 1 and 2), as expected if form drag influences the flow. When the original data set was reanalyzed, using thinner averaging intervals in the upper portion of the profile and also incorporating both upward and downward traverses, it too shows two distinct logarithmic slopes. (In the original study, only downward traverses were used.) Although deviation from a single logarithmic form is not necessarily large, the slope of the logarithmic regression is significantly different in the two regions, implying that the turbulent stress above is significantly larger than it is nearer the bed.

This experiment represents the first time in a natural environment that continuous profiles of current velocity have been obtained down to the sediment-water interface. We find that estimates of bed shear stress, using sensors located farther than 15 cm from the bed, were significantly influenced by the presence of form drag and that sediment entrainment calculations, using such estimates, would be based on stresses more than 4 times the true stress at the bed.

## THE EXPERIMENT

The experiment was carried out October 11–12, 1978, at 45°20'N (199 m total water depth) on the Oregon shelf. The surface sediment was silty sand [*Runge*, 1966]. Profiling heated-thermistor velocity sensors were mounted on a 2-m-high tripod placed on the seafloor. Most data come from an 18-hour deployment. Some additional data were obtained in a 4-hour deployment. A data acquisition system on the tripod sampled each thermistor every 1.5 s during the 18-hour deployment and every 0.38 s during the 4-hour deployment. Additional instrumentation included profiling and stationary temperature sensors, stationary heated-thermistor sensors, Savonius rotors, a 25-cm path-length beam trans-

[1] Now at Department of Oceanography, Dalhousie University, Halifax, Nova Scotia, Canada B3H 4JH.



Paper 1C1841.
0148-0227/82/001C-1841$01.00

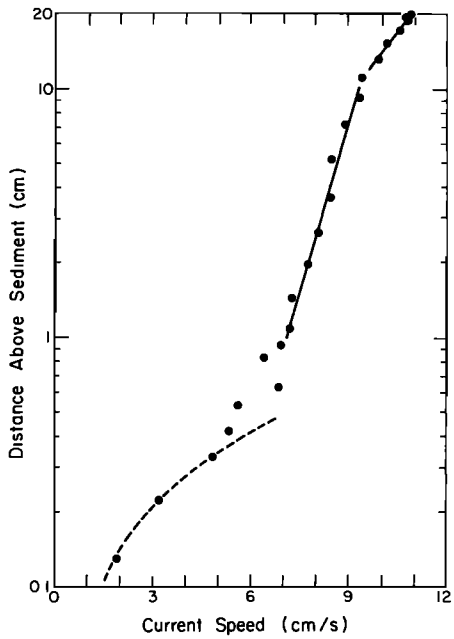


Fig. 1. Typical mean velocity profile for the October 1978 experiment. The dashed line represents a linear fit in the viscous sublayer. The solid lines represent fits to the data in the lower and upper logarithmic regions of the velocity profile. The region between the dashed line and the lower solid line is the so-called 'buffer' region where the velocity profile obeys neither a linear nor a logarithmic law. (Interval number 4 of Table 1.)

missometer, a high-resolution pressure transducer, and a time-lapse motion picture camera that monitored the condition of the sensors.

Current was supplied to each heated thermistor to heat it approximately 20°C above the water temperature. The temperature achieved by the thermistor depends on the power dissipated in it and on the heat transferred away by the water flowing past it. Because the calibration is a function of both the water temperature and the orientation of the flow with respect to the thermistor, each thermistor was post-calibrated at the temperatures and flow directions observed during the experiment. Calibrations were performed by towing the thermistor in a 1-m radius annular channel. The power dissipated in the thermistor per degree change in temperature was related to the flow velocity by

$$P/\Delta T = A + BU^N \tag{3}$$

where $P$ is the power dissipated in the thermistor, $\Delta T$ is its temperature rise, $U$ is the speed, and $A$, $B$, and $N$ are experimentally determined. Inversion of this formula allows the calculation of speed from measurements of $P/\Delta T$, which is computed from the output of a bridge circuit. By using (3) with empirically determined $A$, $B$, and $N$, speed can be determined within 0.1 cm/s in the laboratory. The heated thermistors measure speed only, flow direction being determined by a small vane.

The heated thermistors were carried up and down by a crank-and-piston mechanism driven by an underwater motor. The mechanism was mounted outside one tripod leg, to provide unobstructed flow through an arc of 300°. Only data from times when the flow was completely unobstructed were analyzed. The profiling period was 1 min, and the vertical travel was 21 cm. During the 4-hour deployment, the thermistors came within a few centimeters of the sediment-water interface, but during the 18-hour deployment the thermistors penetrated the sediment 0.3 cm. The vertical position of the sensors was determined by a potentiometer connected to the motor shaft. Calibration with a dial indicator showed that the vertical position was known to within 0.03 cm. The location of the sediment-water interface was taken to be the zero-velocity intercept of the linear velocity profile within the viscous sublayer. Although the thermistors did not always penetrate the sublayer during the 4-hour deployment, they did penetrate it during one interval of very low current, allowing the interface position to be determined.

## DATA ANALYSIS

Mean profiles were constructed by averaging over time intervals 28–44 min long, each interval containing many traverses. Intervals were chosen for steadiness of speed and direction. Within 1.2 cm of the sediment the traverse was divided into layers 0.1 cm thick for averaging; above 1.2 cm, the averaging layers were 1–2 cm thick. The mean for each layer was determined by averaging all measurements within it during the repeated traverses. Before averaging, the effect of the profiler's vertical velocity was removed by vector subtraction from the measured velocity. Corrections for sampling error due to variability of the large-scale flow were made by using measurements from a stationary sensor 20 cm above the sediment [*Badgley et al.*, 1972].

The shear in the viscous sublayer was determined by linear regression, and bed stress was computed by using the relationship

$$\tau_b = \rho\nu\partial\bar{U}/\partial z \tag{4}$$

where $\rho$ and $\nu$ are the density and kinematic viscosity of sea water. Logarithmic regression in the lower segment of the logarithmic region yielded estimates of $z_0$ and $k$, assuming equality of the sublayer stress with that in the lower logarithmic layer. It should be emphasized that in hydrodynamically

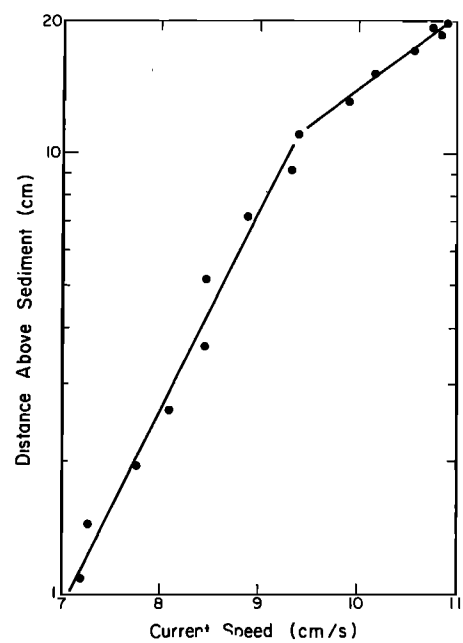


Fig. 2. Same data as Figure 1, plotted with a scale that emphasizes the logarithmic regions of the velocity profile.

TABLE 1. Friction Velocities, Roughness Lengths, and von Karman's Constants for Individual Data Intervals

| Data Interval | Flow Direction* | $u^*$ (sublayer), cm/s | $k$ (for lower log region) | $z_0$, cm | $Z_0$, cm | $U_*$ (upper log region), cm/s |
|---|---|---|---|---|---|---|
| 1 | 90 | 0.27 | 0.40 ± 0.04 | $2.5 \times 10^{-3}$ | 0.29 | 0.62 |
| 2 | 90 | 0.30 | 0.88 ± 0.24 | $3.8 \times 10^{-4}$ | 1.39 | 0.62 |
| 3 | 270 | 0.51 | 0.41 ± 0.05 | $6.2 \times 10^{-4}$ | 0.080 | 1.00 |
| 4 | 270 | 0.47 | 0.49 ± 0.03 | $6.6 \times 10^{-4}$ | 0.27 | 1.02 |
| 5 | 110 | 0.19 | 0.53 ± 0.10 | $2.5 \times 10^{-4}$ | 1.23 | 0.62 |

*Flow direction is given with respect to tripod coordinate system.

smooth flow $z_0$ reflects only the sublayer thickness and is not determined by the grain size of the sediment [*Chriss and Caldwell,* 1981].

Logarithmic regression in the upper segment yielded estimates of $Z_0$ and $U_*$ (Table 1). For the latter calculation, $k$ in the top segment was taken to be 0.4. A second sensor produced qualitatively similar segmented profiles. Detailed analysis of this data was discontinued, however, because large and variable $k$ estimates (0.8–1.6), occasional negative shears, and evidence of intermittent sensor malfunction indicate that these data may not be reliable.

Before considering the significance of the segmentation of the profiles, we consider two questions: (1) Are these profiles representative of this region, or do they merely reflect some unusual conditions in the immediate area of the tripod; and (2) is the segmentation an artifact of our measuring system? The question of representativeness can be approached by considering that although all of the data of Table 1 and Figures 1 and 2 came from the 18-hour deployment, similar segmented profiles were obtained during the 4-hour deployment. Because of the small chance of setting the tripod down in the same spot twice, these results must be representative to some extent. To answer the second question, we consider profiles obtained at the beginning of each deployment. As the tripod was lowered to the seafloor, the profiler mechanism was operating but in a retracted position to prevent damage to the sensors. A timed release lowered the mechanism to the sediment 20–40 min later. So at the beginning of each deployment the sensors were being traversed between 26 and 47 cm above the sediment. These profiles show no segmentation, evidence that the profiler mechanism itself does not cause it.

Although *Smith* [1977] and *Grant and Madsen* [1979] suggest that, for combined waves and current near the sea bed, the slope of the mean velocity profile above the wave boundary layer may differ from that closer to the bed, it is unlikely that the segmented profiles in our study represent such an effect. The thickness of the viscous wave boundary layer, $\delta_w = (\nu/\omega)^{1/2}$, would have been only 0.19 cm for the 15-s waves observed, and hence the top of the wave boundary layer would have been well within the viscous sublayer and almost 2 orders of magnitude closer to the bed than the 'kinks' in our profiles. A Reynolds number $U_0\delta_w/\nu$ formed from $\delta_w$ and the orbital velocity $U_0$ (3.5 cm $s^{-1}$) is only 44 and hence is consistent with the assumption of a viscous wave boundary layer. (The smallest Reynolds number at which a turbulent wave boundary layer might exist is 113–250 [*Smith,* 1977].)

Furthermore, although wave orbital velocities to 3.5 cm $s^{-1}$ were obvious during the 18-hour deployment, no oscillatory motion was observed in the 4-hour deployment. Segmented profiles were found in both deployments, further evidence that the segmentation is not caused by surface waves.

## DISCUSSION

Although the shape of the profiles suggests that form drag was significant, we have no direct information about bedforms or other small-scale features in the area. We tried to obtain stereo photographs with a borrowed camera system, but were foiled by a faulty triggering mechanism. The time-lapse camera on the tripod did obtain low-quality photographs of the bed, but, because the field of view was restricted to 1 $m^2$ and because the lighting was optimized for sensor observation, the absence of obvious features in these photographs is not conclusive. Features just outside the field of view could have significant influence on the flow. Because the photographic information is inconclusive, estimates of the size and spacing of roughness elements must come from analysis of the velocity profiles themselves. In a later section of this paper, we will, however, present some photographic evidence from an area 65 km to the south.

The following analysis is restricted to the 18-hour deployment because during the shorter deployment the currents were extremely small so the observations are less accurate.

### *Estimates of Roughness Element Geometry*

*Elliot* [1958] derives the following expression for the growth of an internal boundary layer following a change in roughness:

$$(\delta_{IBL}/z_0) = a(x/z_0)^{0.8} \tag{8}$$

where $\delta_{IBL}$ is the thickness of the internal layer a distance $x$ from a change in the surface roughness, $z_0$ is the roughness length for the internal layer, and $a$ depends on the ratio of $z_0$ to the roughness length, $Z_0$, for the flow outside the internal layer:

$$a = 0.75 - 0.03 \ln(z_0/Z_0) \tag{9}$$

As was noted by *Arya* [1975], Elliot's model is supported by measurements over a hot runway [*Elliot,* 1958] and also by the observations of *Bradley* [1968] under near-neutral conditions and by the results of a second-order closure model by *Rao et al.* [1974].

*Arya* [1975] suggests that Elliot's model may also apply to the growth of an internal boundary layer in the region

TABLE 2. Estimated Distances From Sensor to Roughness Elements

| Data Interval | Flow Direction | $z_*$, cm | $x$, cm |
|---|---|---|---|
| 1 | 90 | 11.3 | 107 |
| 2 | 90 | 14.3 | 200 |
| 3 | 270 | 10.8 | 142 |
| 4 | 270 | 10.9 | 135 |
| 5 | 110 | 14.3 | 220 |

Calculated using measured $z_*$, $z_0$, and $Z_0$ values and the theory of *Elliot* [1958].

between large-scale roughness elements and, like *Smith* [1977] and *Smith and McLean* [1977], uses Elliot's results to model the influence of form drag on velocity profiles. The position $z_*$ of the kink in the profiles is assumed to represent the local thickness ($\delta_{IBL}$) of the developing internal boundary layer. Applying the model, we estimate $x$ from determinations of $z_0$, $Z_0$, and $z_*$ from our profiles. These estimates (Table 2) suggest that elements capable of explaining our velocity profiles would not have been within our camera's field of view. It is unlikely that oscillatory ripple marks [*Komar et al.*, 1972] are responsible, because the maximum ripple spacing reported by Komar et al. was only 21 cm, 5–10 times smaller than our estimates. *Miller and Komar* [1980] suggest that the maximum ripple length is a function of grain size. Using their results and the grain size in our area, we calculate that the maximum ripple spacing would have been less than 10 cm.

Height estimates for the elements can be obtained from a model developed by *Arya* [1975] for estimation of $Z_0$ and $\tau_t$ over Arctic pack ice. Because we lack the detailed topographic information required to verify the assumptions of the model, we will apply the model formally but interpret the results of our analysis with some caution. Arya finds

$$\ln(Z_0/z_0) = 4/5[\ln(h/z_0) + \ln(1/\lambda - b/h - B/h)] \cdot [1 - (k_u/k_L)\{1 - m\lambda + (C_D\lambda/2k_L^2)(\ln h/z_0)^2\}^{-1/2}] \quad (10)$$

Here $h$ is the height of the elements; $\lambda$ is the ratio of $h$ to their spacing $s$; $b$ is their width; and $B$ is the sum of the widths of the regions of separated flow that may exist around the roughness elements. Over streamlined elements the flow may not separate, and $B$ may be neglected. $C_D$ is a drag coefficient that relates the form drag on the element to the mean velocity (at $z = h$) of the upstream flow:

$$F_D = \frac{1}{2} C_D \lambda \rho \bar{U}(h)^2 \quad (11)$$

Here $F_D$ is the form drag per unit area of the bed and $\rho$ is the density of the fluid. The constant $m$ in (10) is taken by Arya to be 20. Equation (10) differs from equation (15) of Arya in not assuming equality of the values of von Karman's 'constants' ($k_L$ and $k_u$) inside and outside the internal boundary layer. We will use (10) because, although our estimates of $k$ are not always 0.4 in the internal layer (Table 1), we have no evidence that $k$ is not 0.4 above. Although deviations of $k_L$ from the commonly accepted value of 0.4 may simply reflect uncorrected sampling or measurement errors in our data, some laboratory data suggests that $k_L$ is not always 0.4 in internal boundary layers between roughness elements [*Paola et al.*, 1980]. Use of (10) allows us to use measured values of $k_L$ while still using 0.4 outside the internal boundary layer.

Although (10) was derived to predict $Z_0$, it can be solved (iteratively) for $h$, using measured values of $Z_0$, $z_0$, and $k_L$ from our profiles, together with estimates of the other quantities. We set $b$ to 70 cm; changing it by 50 cm changes $h$ by only 10%. We set $B$ to zero, but with our data the model is not very sensitive to the value of $B$. The spacing $s$ was taken to be 348 cm based on estimates of $x$ (Table 2) for flow directions 180° apart. Because of the lack of information about element shape, the choice of $C_D$ is not obvious, so we have used a range of values from the literature [*Arya*, 1973; *Smith and McLean*, 1977].

The results of these calculations (Table 3) yield plausible element heights for the larger drag coefficients. (We have excluded heights calculated for the smaller drag coefficients for some of the intervals because these calculated heights violate an assumption of the model, which is that $\lambda$ is less than 1/m.) We conclude that if the model is applicable, flow over roughness elements 4 to 17 cm high with drag coefficients of 0.8 or larger could generate our velocity profiles.

### *Photographic Evidence from the Oregon Shelf*

As was mentioned earlier, we have no photographic information about small-scale bottom topography in the area of the study. We do, however, have some information from a large number of bottom photographs obtained 65 km to the south, from an area of the same water depth (200 m) and similar sediment texture. These photographs, furnished by Andrew Carey of Oregon State University, were obtained as part of a study of the sampling efficiency of beam trawls. A single camera was mounted just ahead of the trawl for the purpose of photographing the sediment prior to sampling. Although current generated bedforms are absent, typical bottom photographs (Figures 3 and 4) reveal two dominant types of biologically related roughness elements. The sea urchins (typically 6–8 cm in diameter) are ubiquitous, although their abundance varies significantly. The 'mounds' represent sediment expelled from burrows that were possibly occupied by polychaete worms. By comparison with the known size of the urchins, the height of the mounds can be estimated to vary from a few centimeters to more than 15 cm. The spacing of the mounds varies greatly from photograph to photograph as well as within a single photograph. In some cases, mounds nearly coalesce and form ridges. Photographs from different years all show features similar to those in Figures 3 and 4. Because the density and height of the roughness elements vary from photograph to photograph, and because stereo photos are not available, it is difficult to

TABLE 3. Roughness Element Heights (cm) Estimated by Applying the Model of *Arya* [1975] and Various Assumptions About the Roughness Element Drag Coefficient ($C_D$)

| Data Interval | Assuming $C_D = 1.00$ | Assuming $C_D = 0.84$ | Assuming $C_D = 0.4$ |
|---|---|---|---|
| 1 | 6.4 | 7.5 | 14.9 |
| 2 | 16.7 | —* | —* |
| 3 | 3.9 | 4.7 | 9.1 |
| 4 | 6.3 | 7.4 | 15.2 |
| 5 | 16.0 | —* | —* |

*Calculated heights have been omitted because they violate the assumptions of Arya's model.

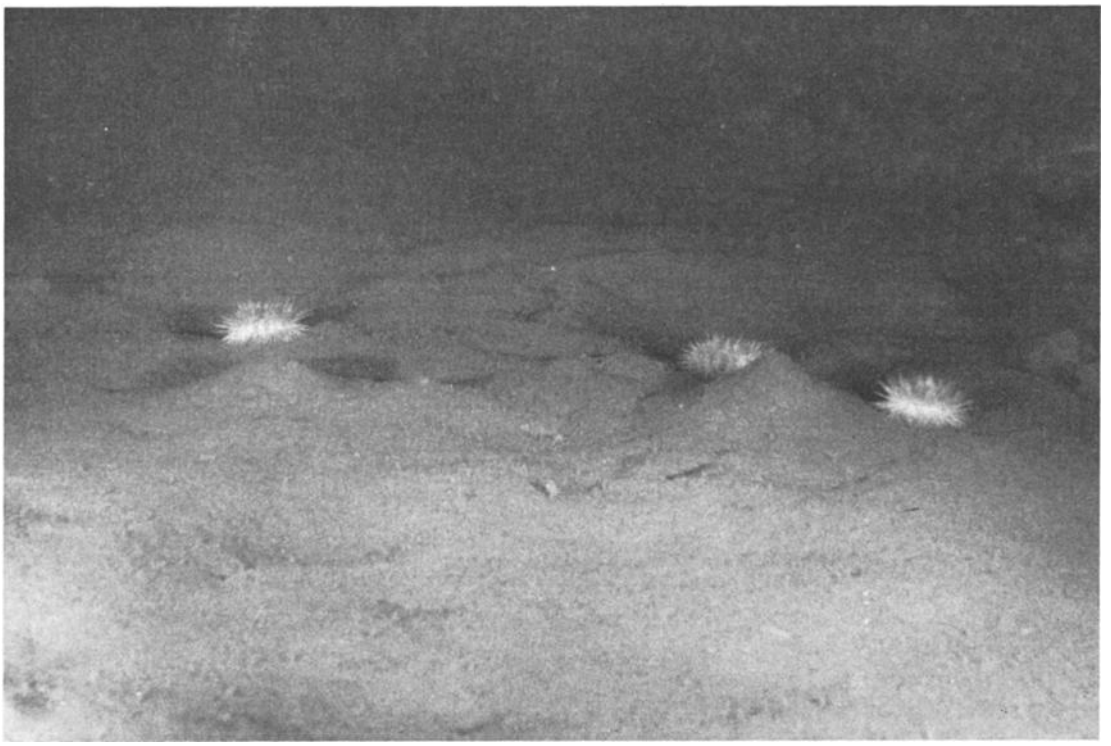

Fig. 3. Photograph representative of those obtained 65 km south of our area of study, in a region of the same water depth (200 m) and similar sediment texture. See text for description.

define a characteristic height or spacing for these features. Although we have no reason to expect significant differences along the 200-m isobath, especially in light of the similar sediment texture, we cannot demonstrate that these features are representative of roughness elements in our area of study. We can only state that the types of features in these photos could be responsible for the form drag that we infer from our current data.

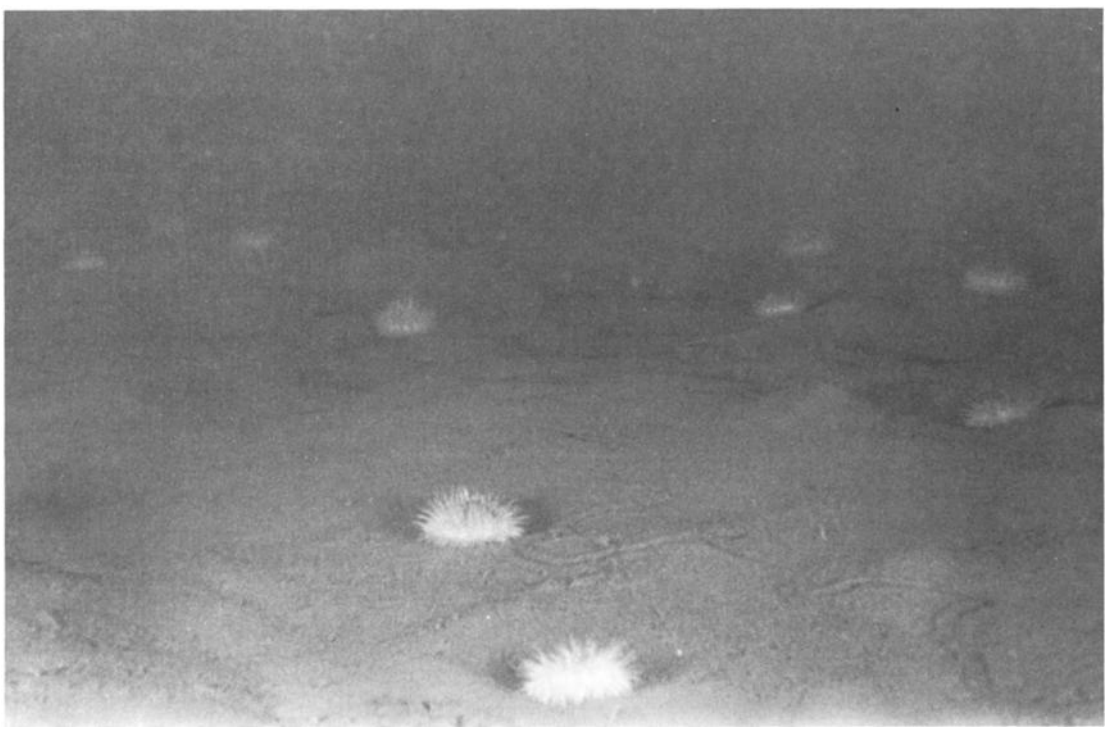

Fig. 4. Additional photograph from the area described in Figure 3.

TABLE 4. Ratio of the Total Stress ($\tau_t$) to the Bed Stress ($\tau_b$)

| Data Interval | $\bar{U}(100)$, cm/s | $u_*$ (sublayer), cm/s | $U_*$ (upper) region), cm/s | $C_{100}$ | $\tau_t/\tau_b$ |
|---|---|---|---|---|---|
| 1 | 9.1 | 0.27 | 0.62 | $4.7 \times 10^{-3}$ | 5.3 |
| 2 | 6.6 | 0.30 | 0.62 | $8.8 \times 10^{-3}$ | 4.3 |
| 3 | 17.8 | 0.51 | 1.00 | $3.2 \times 10^{-3}$ | 3.8 |
| 4 | 15.0 | 0.47 | 1.02 | $4.6 \times 10^{-3}$ | 4.8 |
| 5 | 6.8 | 0.19 | 0.62 | $8.2 \times 10^{-3}$ | 10.6 |

Also shown are drag coefficients ($C_{100}$) calculated using the data from the upper logarithmic region.

*Techniques Used to Estimate Bed Stress*

It is common practice in sediment-transport studies to measure the mean current some distance above the bed (typically 100 cm) and to estimate the bed stress from the quadratic law:

$$\tau_b = C_{100}\rho[\bar{U}(100)]^2 \quad (12)$$

Here $\tau_b$ is taken to be the bed stress, and $C_{100}$ is a dimensionless drag coefficient [*Sternberg*, 1968, 1972; *McCave*, 1973; *Ludwick*, 1975; *Komar*, 1976]. Because $C_{100}$ is commonly determined by a logarithmic profile technique in which the velocity profile is measured well above the bed, the measured stress and therefore the calculated $C_{100}$ may be influenced by form drag. If the goal of a study is to obtain an estimate of skin friction for use in entrainment or transport calculations, and if form drag is significant, use of (12) may yield $\tau_b$ considerably larger than the stress influencing the near-bed sediment transport. The same statement can obviously be made about Reynolds stress estimates if based on measurements a significant distance from the bed. The above ideas are not new but rather are consequences of concepts presented most recently by *Smith* [1977] and *Smith and McLean* [1977]. Our experiment, however, provides the first, though somewhat limited, data set from the ocean that demonstrates the degree to which the local bed stress may be overestimated. Were it not for our measurements within 15 cm of the bed, our measurements of $U_*$ from the top portion of our profiles would have been assumed to represent the friction velocity at the bed, and the relatively large $Z_0$ values calculated from the top portion of the profiles might have been interpreted to imply that the flow was not hydrodynamically smooth and that a viscous sublayer did not exist. In contrast, our data clearly demonstrate that this interpretation cannot be justified without evidence from velocity profiles closer to the sediment. For example, the calculation by *Weatherly and Wimbush* [1980] of $U_* = 0.66$ cm/s and $Z_0 = 0.49$ cm based on profiles obtained with sensors located between 18 and 565 cm above the sediment does not necessarily indicate that a viscous sublayer did not exist or that the $U_* = 0.66$ cm/s value represents the skin friction or the stress at the bed. Without near-bed velocity profiles it is difficult to evaluate their conclusion that the critical erosion stress ($u_* = 0.6$ cm/s) was exceeded, particularly because of the possible influence of the current ripples shown in their Figure 2.

Although the flow during our experiment was hydrodynamically smooth in the sense that a viscous sublayer did always exist, drag coefficients (Table 4) computed from the extrapolated velocity at 100 cm (using the $U^*$ values for the upper logarithmic layer) fall within the range other workers cite as typical for hydrodynamically rough flow. For example, the data of *Sternberg* [1972] yield values of $C_{100}$ that, for fully rough flow, lie between $10^{-3}$ and $10^{-2}$ with a mean of $3.1 \times 10^{-3}$, while the data in *Weatherly and Wimbush* [1980] can be used to calculate a value of $5.6 \times 10^{-3}$ for $C_{100}$. Our study shows that large $Z_0$ values and large $C_{100}$ values, if not derived from measurements just above the sediment-water interface, may reflect the influence of form drag on the boundary layer flow, and use of these values in calculating the bed stress may significantly overestimate the actual stress at the bed. The ratio of the 'total stress' ($\tau_t$), calculated from the upper portion of our velocity profiles, to the sublayer stress (Table 4) shows that entrainment or near-bed transport calculations based on velocity profile (or Reynolds stress) measurements more than 15 cm above the bed would in our case have been based on stress estimates more than 4 times too large.

*How Representative Are Our Data?*

It must be emphasized that the data that form the basis for this paper were obtained during one experiment conducted at 199 m water depth on the Oregon shelf during October 1978 and can only be assumed to reflect the flow conditions during this experiment. While form drag may be of equal (or greater) importance in other shelf and deep-sea locations, we lack the direct evidence necessary to demonstrate this. In the subsequent experiments (April and June 1979), we restricted the profiler motion to 6 cm to increase the resolution of the viscous sublayer and so-called buffer layer. While doing so allowed us to construct mean velocity profiles by using averaging times as short as 10 min, it prevents us from examining these profiles for evidence of form drag. However, data from the sublayer profiler coupled with data from a Savonius rotor 59 cm above the sediment during the June 1979 experiments (in 90 and 180 m water depths) are consistent (within the accuracy of the rotor) with the assumption of a constant stress layer extending from the sediment up to 59 cm [*Chriss and Caldwell*, 1981]. These data suggest that form drag did not significantly influence the flow during the June 1979 experiment.

Clearly, future experiments must incorporate both sublayer profiling (to determine bed stress) and profiling of the lower logarithmic region to determine the extent to which bottom boundary layer flow is influenced by form drag in various environments. These experiments must include quantitative determination of the small-scale topography, especially if drag-partition models are to be tested.

## CONCLUSIONS

Above the viscous sublayer, the velocity profiles observed during this experiment consisted of two distinct regions, each characterized by a different logarithmic velocity pro-

file. Applying the models of *Elliot* [1958] and *Arya* [1975] to these data, we conclude that the influence of form drag on boundary layer flow over sparse roughness elements could produce the velocity structure that we have observed. When form drag is significant, the use of the logarithmic profile or Reynolds stress techniques, if based on flow measurements obtained more than a few tens of centimeters from the bed, may yield stress estimates several times larger than the bed stress. If the goal of a study is to obtain bed stress estimates for use in sediment transport or entrainment calculations, such errors may be unacceptable.

Large values of the roughness parameter ($Z_0$) and the drag coefficient ($C_{100}$), if based on measurements at substantial distances above the bed, do not rule out the existence of a viscous sublayer at the sediment-water interface. This observation is significant, not only for sediment and momentum transport problems, but also because the presence or absence of a viscous sublayer may have important implications for the vertical transport of heat and chemical species at the sediment-water interface.

*Acknowledgments.* Particular appreciation is expressed to Mark Matsler (profiler development), Steve Wilcox (electronics design), Stuart Blood (software development), Mike Brown (sensor construction), and Milo Clauson (mechanical design). Stuart Eide and Tom Dillon generously furnished advice and assistance and the captain and crew of the R/V *Wecoma* were extremely helpful in accommodating a complex mooring procedure. Particular thanks are extended to Priscilla Newberger who assisted with calibrations and helped run the experiment at sea. This material is based upon work supported by the National Science Foundation under grant OCE-7918904

## REFERENCES

Arya, S. P. S., Contribution of form drag on pressure ridges to the air stress on arctic ice, *J. Geophys. Res., 78,* 7092–7099, 1973.

Arya, S. P. S., A drag partition theory for determining the large-scale roughness parameter and wind stress on the arctic pack ice, *J. Geophys. Res., 80,* 3447–3454, 1975.

Badgley, F. I., C. A. Paulson, and M. Miyake, *Profiles of Wind, Temperature, and Humidity over the Arabian Sea,* p. 42, University of Hawaii Press, 1972.

Bradley, E. F., A micrometeorological study of velocity profiles and surface drag in the region modified by a change in surface roughness, *Q. J. R. Meteorol. Soc., 94,* 361–379, 1968.

Caldwell, D. R., and T. M. Chriss, The viscous sublayer at the sea floor, *Science, 205,* 1131–1132, 1979.

Chriss, T. M., and D. R. Caldwell, Universal similarity and the thickness of the viscous sublayer at the ocean floor, submitted to *J. Geophys. Res.* 1981.

Einstein, H. A., The bed-load function for sediment transportation in open channel flows, *Tech. Bull. 1026,* U.S. Dept. of Agriculture, Washington, D. C., 1950.

Einstein, H. A., River sedimentation, in *Handbook of Applied Hydrology,* edited by Ven Te Chow, McGraw-Hill, New York, 1964.

Elliot, W. P., The growth of the atmospheric internal boundary layer, *Eos Trans. AGU, 39,* 1048–1054, 1958.

Grant, W. D., and O. S. Madsen, Combined wave and current interaction with a rough bottom, *J. Geophys. Res., 84,* 1797–1808, 1979.

Komar, P. D., Boundary layer flow under steady unidirectional currents, in *Marine Sediment Transport and Environmental Management,* edited by D. J. Standley and D. J. P. Swift, John Wiley, New York, 1976.

Komar, P. D., R. H. Neudeck, and L. D. Kulm, Observations and significance of deep-water oscillatory ripple marks on the Oregon continental shelf, in *Shelf Sediment Transport,* edited by D. J. P. Swift, D. B. Duane and O. H. Pilkey, p. 601–619, Dowden, Hutchinson and Ross, Stroudsberg, Pa., 1972.

Ludwick, J. C., Variations in boundary drag coefficient in the tidal entrance to Chesapeake Bay, Virginia, *Mar. Geol., 19,* 19–28, 1975.

McCave, I. N., Some boundary-layer characteristics of tidal currents bearing sand in suspension, *Mém. Soc. R. Sci. Liège, 6,* 107–126, 1973.

Miller, M. C., and P. D. Komar, Oscillation sand ripples generated by laboratory apparatus, *J. Sedimentol. Petrol., 50,* 173–182, 1980.

Paola, C., G. Gust, and J. Southard, Flow structure and skin friction over two-dimensional ripples (abstract), *Eos Trans. AGU, 61,* 989–990, 1980.

Rao, K. S., J. C. Wyngaard, and O. R. Coté, The structure of the two-dimensional internal boundary layer over a sudden change of surface roughness, *J. Atmos. Sci., 31,* 738–746, 1974.

Runge, E. J., Continental shelf sediments, Columbia River to Cape Blanco, Oregon, Ph.D. thesis, Oregon State Univ., Corvallis, 1966.

Smith, J. D., Modeling of sediment transport on continental shelves, in *The Sea,* vol. 6, edited by E. D. Goldberg, John Wiley, New York, 1977.

Smith, J. D., and S. R. McLean, Spatially averaged flow over a wavy surface, *J. Geophys. Res., 82,* 1735–1746, 1977.

Sternberg, R. W., Friction factors in tidal channels with differing bed roughness, *Mar. Geol., 6,* 243–260, 1968.

Sternberg, R. W., Predicting initial motion and bedload transport of sediment particles in the shallow marine environment, in *Shelf Sediment Transport,* edited by D. J. P. Swift, D. B. Duane and O. H. Pilkey, p. 61–82, Dowden, Hutchinson and Ross, Stroudsberg, Pa., 1972.

Weatherly, G. L., and M. Wimbush, Near-bottom speed and temperature observations on the Blake-Bahama Outer Ridge, *J. Geophys. Res., 85,* 3971–3981, 1980.

(Received Februray 11, 1981;
revised November 23, 1981;
accepted December 3, 1981.)